In-plane magnetic field-induced skyrmion crystal in frustrated magnets with easy-plane anisotropy

Satoru Hayami
Department of Applied Physics, The University of Tokyo, Tokyo 113-8656, Japan

(Received 4 May 2021; revised 9 June 2021; accepted 10 June 2021; published 17 June 2021)

We theoretically investigate the instability toward a skyrmion crystal (SkX) in frustrated triangular magnets. By performing simulated annealing and Monte Carlo simulations, we show that a frustrated spin model with easy-plane single-ion anisotropy exhibits a SkX in an in-plane external magnetic field. The emergent SkX is a counterpart of that induced by easy-axis anisotropy in an out-of-plane magnetic field, both of which show the topological Hall effect. We also find that a variety of multiple-Q states distinct from the SkX are stabilized in the presence of easy-plane anisotropy. Our results provide a possibility to realize a SkX in easy-plane frustrated magnets by applying an in-plane magnetic field to in-plane cycloidal spiral magnets.

DOI: 10.1103/PhysRevB.103.224418

I. INTRODUCTION

Magnetic frustration, which is a conflict of competing interactions owing to a geometrical lattice structure in magnetic systems, is one of the central topics in condensed matter physics [1]. Such a competing interaction gives rise to exotic states, such as a spin liquid [2–5], spin ice [6–9], spin supersolid [10–12], and so on. It also induces complicated magnetic orderings with noncollinear [13–16] and noncoplanar spin textures [17–21]. The various magnetic ordered parameters cause fascinating physical phenomena, such as the magnetoelectric effect in noncollinear magnets [22–25] and the topological Hall effect in noncoplanar magnets [26–28].

Among them, spiral magnetic orderings in frustrated magnets have long been studied in various fields such as spintronics and multiferroics [29]. In particular, a magnetic skyrmion crystal (SkX) by superposing multiple spiral waves has been attracting great interest [30,31]. Although the SkX has been mainly investigated in chiral magnets with the Dzyaloshinskii-Moriya (DM) interaction [32–36], it also appears in frustrated magnets [37–44] and in itinerant magnets [45–49] in an external magnetic field along the out-of-plane direction. As the latter mechanisms do not require inversion symmetry breaking in the lattice structure, the resultant SkX can exhibit different features from that in chiral magnets; in the case of frustrated magnets, it was demonstrated that characteristic dynamics emerge due to the degeneracy in terms of helicity and associated Goldstone modes [39,50–53]. However, the materials hosting a SkX stabilized by a frustrated exchange interaction are rare compared to those by a DM interaction [54–58]. It is desirable to examine other mechanisms for a SkX in frustrated magnets to stimulate experimental observations.

In the present paper, we investigate the stability of a SkX in frustrated magnets with easy-plane anisotropy. By performing simulated annealing and Monte Carlo simulations for a frustrated Heisenberg model on a triangular lattice, we find that an in-plane magnetic field stabilizes the SkX in easy-plane magnets, which have often been discussed in the presence of the DM interaction [59–62]. Although this SkX is similar to the one that emerges in a system with easy-axis anisotropy in an out-of-plane magnetic field, there is a difference in the symmetry; easy-plane anisotropy combined with an in-plane magnetic field breaks the threefold rotational symmetry of the triangular lattice, while an easy-axis one with an out-of-plane magnetic field does not. Reflecting such a difference, the skyrmion core is elliptically deformed. Moreover, we find a triple-Q coplanar state, which has an in-plane spin texture similar to that in a SkX but without the z-spin component, for strong easy-plane anisotropy. Our results will encourage further experimental exploration of the SkX when an in-plane magnetic field is applied to an in-plane cycloidal spiral state stabilized at zero field.

The rest of the paper is organized as follows. In Sec. II, we present a localized spin model with a frustrated exchange interaction and easy-plane anisotropy. We also show an effective model of the localized spin model which takes into account the dominant interactions in momentum space. In Sec. III, we discuss a low-temperature magnetic phase diagram of the effective model by performing simulated annealing. We find a SkX and triple-Q states under an in-plane magnetic field. We demonstrate that the SkX is also stabilized at finite temperatures by performing Monte Carlo simulations in Sec. IV. Section V is devoted to a summary.

II. MODEL

We consider a frustrated Heisenberg model on a two-dimensional triangular lattice. The model Hamiltonian is given by

$$\mathcal{H} = \sum_{\langle ij \rangle} J_{ij} \boldsymbol{S}_i \cdot \boldsymbol{S}_j - A \sum_i \left(S_i^z\right)^2 - H^x \sum_i S_i^x, \qquad (1)$$

where $\boldsymbol{S}_i$ is the classical localized spin with $|\boldsymbol{S}_i| = 1$. The first term is the isotropic exchange interaction between i and j spins. We consider a ferromagnetic interaction between the nearest-neighbor spins $J_1 < 0$ and an antiferromagnetic interaction between the third-nearest-neighbor spins $J_3 > 0$.

We take $J_1 = -1$ as the energy unit of the model in Eq. (1). The second term represents single-ion anisotropy, where we focus on easy-plane spin anisotropy ($A < 0$). The third term represents the Zeeman coupling to an in-plane external magnetic field with a magnitude H^x. We here neglect long-range dipole-dipole interactions, which can be a source of the SkX [63–66], by supposing that their effect is small.

The ground state of the model in Eq. (1) without H^x is obtained by considering the Fourier transform of the first term, which is given by $\sum_{\boldsymbol{q}} J_{\boldsymbol{q}} \boldsymbol{S}_{\boldsymbol{q}} \cdot \boldsymbol{S}_{-\boldsymbol{q}}$ with

$$J_{\boldsymbol{q}} = 2J_1\left[\cos q_x + \cos\left(\frac{q_x}{2} + \frac{\sqrt{3}q_y}{2}\right) + \cos\left(\frac{q_x}{2} - \frac{\sqrt{3}q_y}{2}\right)\right] + 2J_3[\cos 2q_x + \cos(q_x + \sqrt{3}q_y) + \cos(q_x - \sqrt{3}q_y)], \tag{2}$$

where the lattice constant is taken as unity. The minimization of $J_{\boldsymbol{q}}$ gives the ground state, which corresponds to the ferromagnetic state for $J_3/|J_1| \leqslant 1/4$ and the single-Q spiral state for $J_3/|J_1| > 1/4$ with a spiral pitch $Q = |\boldsymbol{Q}| = 2\cos^{-1}[(1 + \sqrt{1 - 2J_1/J_3})/4]$. Hereafter we focus on a situation where the single-Q spiral state is the ground state for $J_3/|J_1| > 1/4$. The spiral plane is arbitrary for $A = 0$, while it is locked in the xy plane for $A < 0$, representing the in-plane cycloidal spiral.

To investigate the instability toward a SkX in an in-plane magnetic field in a simplified way, we also consider the effective model in Eq. (1) by extracting the dominant $\boldsymbol{q}$ contributions, which is written as

$$\mathcal{H}^{\rm eff} = \sum_{\nu} \tilde{J} \boldsymbol{S}_{\boldsymbol{Q}_\nu} \cdot \boldsymbol{S}_{-\boldsymbol{Q}_\nu} - A \sum_i \left(S_i^z\right)^2 - H^x \sum_i S_i^x, \tag{3}$$

where the first term is simplified by ignoring the contributions from the interaction except for $\boldsymbol{Q}_\nu$. As we focus on the single-Q spiral state for $J_3/|J_1| > 1/4$, we consider three $\boldsymbol{Q}_\nu$ ($\nu = 1-3$) to satisfy the sixfold rotational symmetry of the triangular lattice, $\boldsymbol{Q}_1 = (Q, 0)$, $\boldsymbol{Q}_2 = (-Q/2, \sqrt{3}Q/2)$, and $\boldsymbol{Q}_3 = (-Q/2, -\sqrt{3}Q/2)$. In other words, we neglect the contributions from the higher harmonics and $\boldsymbol{q} = \boldsymbol{0}$ components in the interactions. The coupling constant $\tilde{J} = J_{\boldsymbol{Q}_\nu}$ is taken as the energy unit in the model in Eq. (3). The second and third terms are the same as Eq. (1). In the following, we examine a low-temperature phase diagram of the effective model in Eq. (3) in Sec. III, and then we investigate a finite-temperature phase diagram of the original model in Eq. (1) in Sec. IV.

III. LOW-TEMPERATURE PHASE DIAGRAM OF EFFECTIVE SPIN MODEL

We investigate the instabilities toward the SkX and other multiple-Q states in the model in Eq. (3) by using the simulated annealing from high temperatures down to low temperatures. The simulations are performed for a system size with $N = 60^2$ based on the standard Metropolis local updates. The scheduling of the annealing is as follows: The temperature is reduced with a rate $T_{n+1} = \alpha T_n$, where T_n is the nth-step temperature ($T_0 = 0.1$–1.0) and $\alpha = 0.999\,995$. We set the final temperature $T = 10^{-4}$, where we perform 10^5–10^6 Monte Carlo sweeps for measurements.

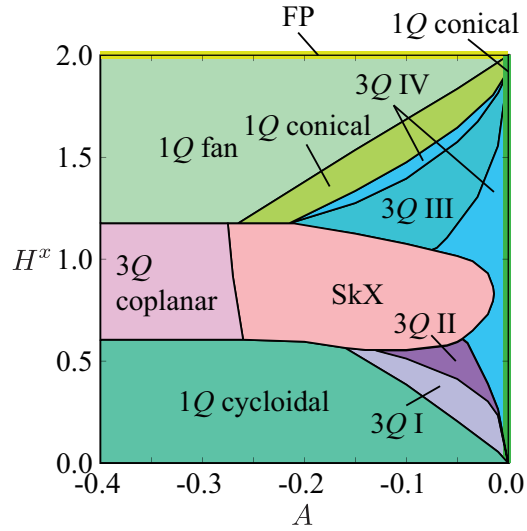

FIG. 1. Magnetic phase diagram of the model in Eq. (3) in the plane of A and H^x. The data are obtained by simulated annealing down to $T = 10^{-4}$ and a system size with $N = 60^2$. FP represents the fully polarized state.

Figure 1 shows the obtained phase diagram on the triangular lattice while varying A and H^x. We choose $Q = 2\pi/6$ without loss of generality. There are nine magnetic phases in addition to the fully polarized state for $H^x \geqslant 2$, which are identified by the spin structure factor as

$$S_s^\alpha(\boldsymbol{q}) = \frac{1}{N}\sum_{j,l} S_j^\alpha S_l^\alpha e^{i\boldsymbol{q}\cdot(\boldsymbol{r}_j - \boldsymbol{r}_l)}, \tag{4}$$

for $\alpha = x, y, z$, and the chirality

$$(\chi_0)^2 = \frac{1}{N^2}\sum_{\mu}\sum_{\boldsymbol{R},\boldsymbol{R}'\in\mu} \chi_{\boldsymbol{R}}\chi_{\boldsymbol{R}'} e^{i\boldsymbol{q}\cdot(\boldsymbol{R}-\boldsymbol{R}')}|_{\boldsymbol{q}=\boldsymbol{0}}, \tag{5}$$

where $\boldsymbol{R}$ and $\boldsymbol{R}'$ stand for the position vectors at the centers of the triangles, and $\mu = (u, d)$ stand for upward and downward triangles, respectively. The local chirality at $\boldsymbol{R}$, $\chi_{\boldsymbol{R}}$, is defined as $\chi_{\boldsymbol{R}} = \boldsymbol{S}_j \cdot (\boldsymbol{S}_k \times \boldsymbol{S}_l)$, where sites j, k, and l form the triangle at $\boldsymbol{R}$ in counterclockwise order. We also calculate the magnetization along the field direction $M^x = (1/N)\sum_i S_i^x$ to distinguish the phases. The H^x dependences of M^x and $(\chi_0)^2$ for $A = -0.05$, -0.2, and -0.4 are shown in Fig. 2. The spin configurations and the spin structure factors in each phase are shown in Figs. 3–5. In the SkX in Fig. 5, we also plot the scalar chirality configuration. The phase diagram is similar to that in the easy-axis magnets in an out-of-plane magnetic field [38,39].

For $A = 0$, the ground state is given by the vertical spiral state whose spiral plane is in the xz or yz plane for an arbitrary H^x, which is denoted as the $1Q$ (transverse) conical state in Fig. 1. When introducing $A < 0$, the system undergoes a transition to the triple-Q state ($3Q$ IV). The spin structure of the $3Q$ IV state is characterized by the single-Q peak in $S_s^x(\boldsymbol{q})$ and the double-Q peaks in $S_s^y(\boldsymbol{q})$ and $S_s^z(\boldsymbol{q})$ with different intensities, as shown in Fig. 4(d). This state is almost characterized by the single-Q conical spiral with $\boldsymbol{Q}_2$ but it is modulated by the second $\boldsymbol{Q}_3$ spiral and the sinusoidal $\boldsymbol{Q}_1$

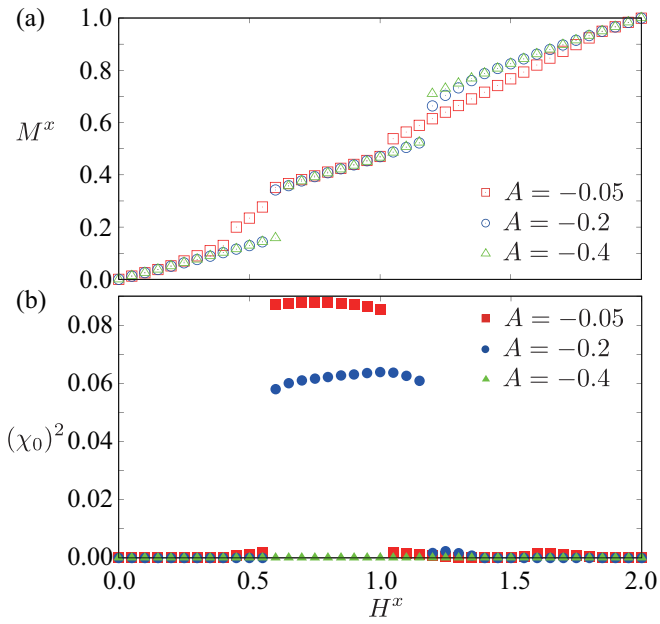

FIG. 2. H^x dependences of (a) the magnetization M^x and (b) the chirality $(\chi_0)^2$ for $A = -0.05$, $A = -0.2$, and $A = -0.4$.

wave. The additional second spiral plane in the $\boldsymbol{Q}_3$ direction is almost circular, i.e., $S^y_s(\boldsymbol{Q}_3) \simeq S^z_s(\boldsymbol{Q}_3)$.

While further increasing $|A|$, the $3Q$ IV state changes into the other multiple-Q states depending on the magnitude of the in-plane magnetic field. In the small H^x region, the $3Q$ IV state is replaced by the $3Q$ I or $3Q$ II state, whose spin configurations and structure factors are shown in Figs. 4(a) and 4(b), respectively. The $3Q$ I state is characterized by the single-Q peak in $S^x_s(\boldsymbol{q})$ and $S^y_s(\boldsymbol{q})$ and the double-Q peaks in $S^z_s(\boldsymbol{q})$, which indicates that the spin configuration is expressed by the in-plane cycloidal spiral modulation in the $\boldsymbol{Q}_1$ direction and the sinusoidal modulations in the $\boldsymbol{Q}_2$ and $\boldsymbol{Q}_3$ directions, as shown in Fig. 4(a). The amplitudes of the $\boldsymbol{Q}_2$ and $\boldsymbol{Q}_3$ are equivalent to each other. On the other hand, the $3Q$ II state has triple-Q peaks in all the components of the spin structure factor, as shown in Fig. 4(b). The $3Q$ II state corresponds to the state where the dominant spiral plane of the $3Q$ I state is tilted from the xy plane so as to include the z component. It is noted that the $3Q$ II state has out-of-plane uniform magnetization perpendicular to the field direction. While further increasing $|A|$, the $3Q$ I state turns into a $1Q$ cycloidal state without showing multiple-Q modulations, whose spin configuration is shown in Fig. 3(a). The xy spiral plane is elliptically deformed due to the presence of a magnetic field.

In the high-field region, the $3Q$ IV state turns into the $3Q$ III state in Fig. 4(c). The spin configuration resembles that in the $3Q$ III state, but the second spiral becomes anisotropic in the $3Q$ IV state. While further increasing $|A|$, reentrant phase transitions occur from the $3Q$ III state to the $3Q$ IV state, and to the $1Q$ conical state. The $1Q$ conical state for $A \neq 0$ has a spiral plane in the yz plane, as shown in Fig. 4(e). The appearance of higher harmonics at $2\boldsymbol{Q}_3$ and $4\boldsymbol{Q}_3$ in $S^x_s(\boldsymbol{q})$ is owing to the elliptical spiral in the yz plane. The increase of $|A|$ in the $1Q$ conical spiral state leads to a transition to the $1Q$ fan state, which is characterized by a single-Q sinusoidal wave in the y-spin component, as shown in Fig. 3(b).

The SkX appears in the intermediate H^x region for a moderate A, as shown in Fig. 1 [67]. This state exhibits a triple-Q spin structure and nonzero χ_0 and is characterized by a quantized skyrmion number of one, which is similar to that induced by easy-axis anisotropy in an out-of-plane magnetic field [38–40]. There are mainly two differences from the previous finding. One is the real-space spin configuration in Figs. 5(a) and 5(b), where the contour shows the z- and x-spin components, respectively. The results obviously indicate that the skyrmion core is characterized by an x-spin component, which is naturally understood due to the presence of H^x. Reflecting that, the spin structure factor in $S^x_s(\boldsymbol{q})$ shows triple-Q peak structures with nearly equal intensities. The other is the breaking of threefold rotational symmetry by an in-plane magnetic field, which is seen in the real-space spin and chirality structures in Figs. 5(a)–5(c) and the spin structure factors in Figs. 5(d)–5(f). However, the topological property of the obtained SkX is the same as that of the SkX with easy-axis anisotropy, since both SkXs have the same skyrmion number of one. Thus, the topological Hall effect is expected to occur in the present system with easy-plane anisotropy.

While increasing $|A|$, the other triple-Q state denoted as the $3Q$ coplanar state is stabilized instead of the SkX in Fig. 1. This state has similar x- and y-spin configurations to the SkX but does not have the z-spin component in Fig. 3(c) [67]. Thus, the x-spin component forms a triangular lattice of a magnetic bubble as in Fig. 5(b), which is regarded as the counterpart of a multiple-Q magnetic bubble in the square and triangular magnets with easy-axis anisotropy [40,68–73]. It is, however, noted that this triple-Q coplanar state has additional triple-Q modulations in $S^y_s(\boldsymbol{q})$ in contrast to the triple-Q collinear bubble in the case of easy-axis anisotropy. This state does not exhibit the topological Hall effect due to the coplanar spin structure.

The behaviors of M^x and χ_0 against H^x are shown for $A = -0.05$, -0.2, and -0.4 in Figs. 2(a) and 2(b), respectively. For easy-plane anisotropy where the SkX emerges in an intermediate field, both M^x and χ_0 show jumps at the critical magnetic field while changing from the SkX to the other states. The small value of χ_0^2 in the regions below and above the SkX is owing to the staggered component of $\chi_{\boldsymbol{R}}$ for the upward and downward triangles (the net component is canceled out). For large easy-plane anisotropy where the $3Q$ coplanar state appears in an intermediate field, M^x also shows a discontinuous behavior with a jump, while keeping $\chi_0 = 0$, as shown in Figs. 2(a) and 2(b). Thus, it is difficult to distinguish which SkX or $3Q$ coplanar state is realized only by the magnetization experiment, which requires Hall conductive measurements.

IV. FINITE-TEMPERATURE PHASE DIAGRAM

We investigate the stability of a SkX at finite temperatures by performing Monte Carlo simulations back to the original spin model in Eq. (1). Monte Carlo simulations are performed for a system size with $N = 60^2$ under periodic boundary conditions. Our simulations are carried out with standard Metropolis local updates. The target temperature is reached by

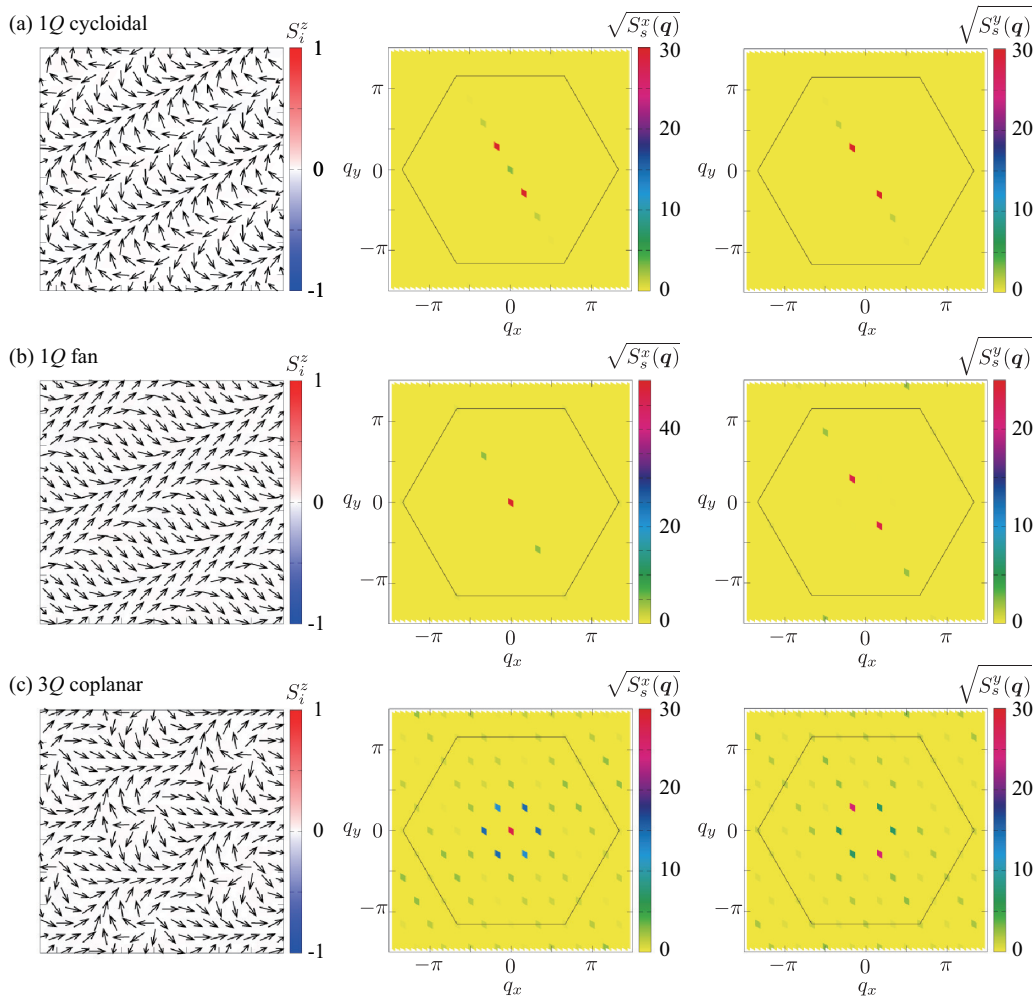

FIG. 3. Left-hand column: Snapshots of the spin configurations in (a) the single-Q ($1Q$) cycloidal spiral state for $A = -0.2$ and $H^x = 0.2$, (b) single-Q ($1Q$) fan state for $A = -0.2$ and $H^x = 1.5$, and (c) triple-Q ($3Q$) coplanar state for $A = -0.4$ and $H^x = 1.0$. The contours show the z component of the spin moment, while the arrows represent the xy components of the spin moment. It is noted that there is no z component in the three states. Middle and right-hand columns: The square root of the x and y components of the spin structure factor, respectively. The hexagons with a solid line show the first Brillouin zone.

simulated annealing over 10^5–10^6 Monte Carlo sweeps from the initial temperature $T_0 = 0.5$–1 to find a low-energy spin configuration, and 10^5–10^6 measurements after equilibration. At each temperature, we perform five independent runs with different initial spin configurations. We take $J_3 = 0.5$ and $A = -0.2$, giving $Q = 2\pi/5$. It is noted that the SkX does not appear for $A = 0$ owing to small Q.

Figure 6 shows the Monte Carlo phase diagram in a plane of temperature T and H^x. The phase boundaries are obtained by a uniform spin susceptibility, specific heat, chirality, and spin structure factor. We find that the SkX is widely stabilized at finite temperatures, whose region extends to the low-temperature region. The appearance of magnetic phases against H^x in Fig. 7 is consistent with the result in Fig. 1: The $1Q$ cycloidal, SkX, $3Q$ III, $1Q$ conical, and $1Q$ fan states are realized while increasing H^x. Among them, we show the spin- and chirality-related quantities in the SkX at $T = 0.175$ and $H^x = 0.38$ in Fig. 7, which are similar to the ones in Fig. 5. Thus, easy-plane anisotropy stabilizes the SkX from zero to finite temperatures as in the case of easy-axis anisotropy, which provides another way to induce the SkX in frustrated magnets.

V. SUMMARY

To summarize, we have theoretically investigated the stability of the SkX on a triangular lattice. We find that the SkX is stabilized in the frustrated Heisenberg model with easy-plane anisotropy in an in-plane magnetic field by simulated annealing and Monte Carlo simulations. The mechanism of the SkX is similar to that by easy-axis anisotropy under an out-of-plane magnetic field, which opens up a possibility to induce the SkX when the in-plane field is applied to the in-plane cycloidal spiral state. Moreover, we obtained a variety of multiple-Q instabilities by the interplay between easy-plane anisotropy and an in-plane magnetic field. Especially, we show that a triple-Q coplanar state with an in-plane spin configuration similar to the SkX but without an out-of-plane spin component is stabilized in the intermediate magnetic field for large easy-plane anisotropy.

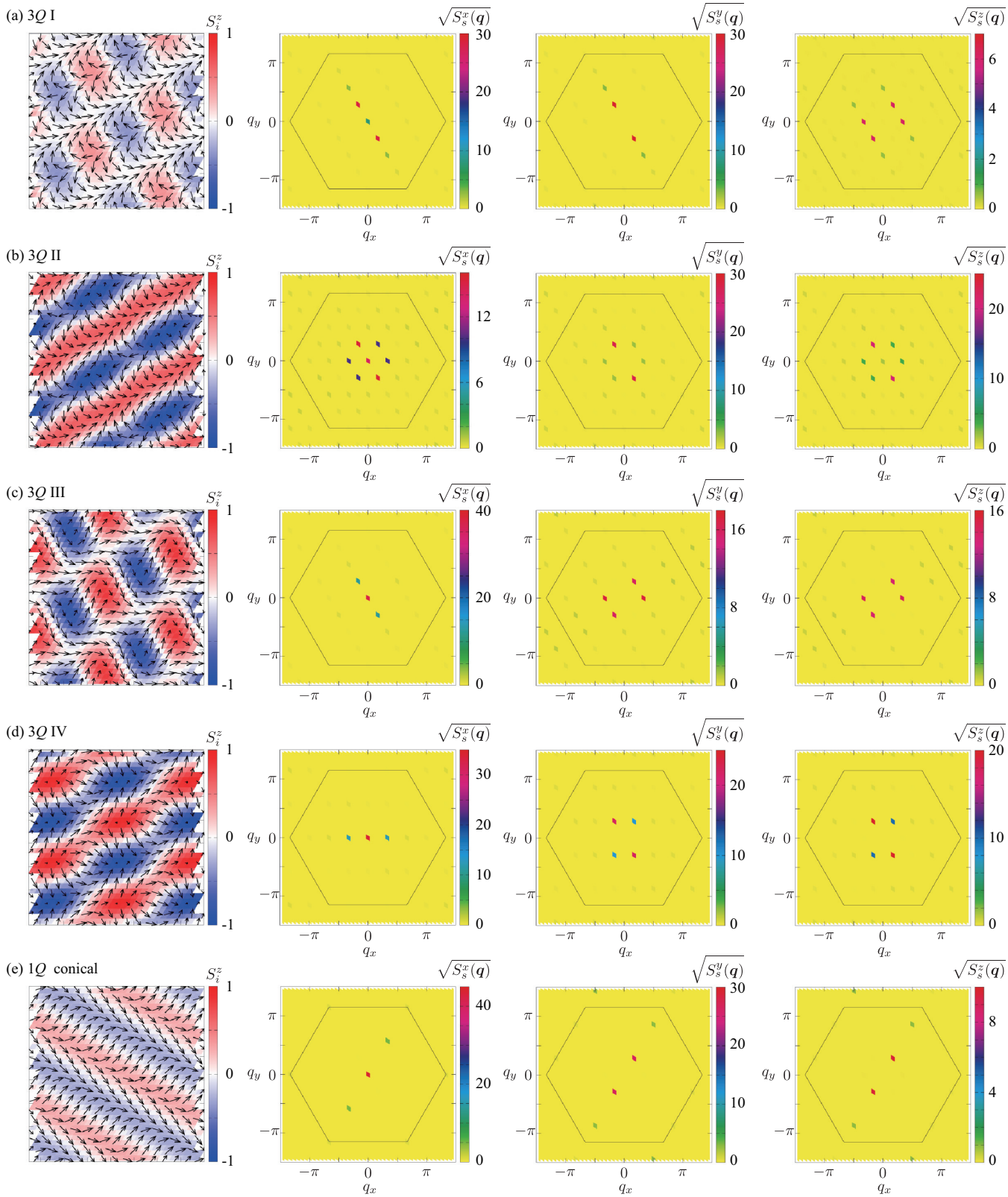

FIG. 4. Left-hand column: Snapshots of the spin configurations in (a) the triple-Q ($3Q$) I state for $A = -0.1$ and $H^x = 0.45$, (b) triple-Q ($3Q$) II state for $A = -0.05$ and $H^x = 0.5$, (c) triple-Q ($3Q$) III state for $A = -0.1$ and $H^x = 1.2$, (d) triple-Q ($3Q$) IV state for $A = -0.05$ and $H^x = 1.1$, and (e) single-Q ($1Q$) conical state for $A = -0.2$ and $H^x = 1.3$. The contours show the z component of the spin moment, while the arrows represent the xy components of the spin moment. Three right-hand columns: The square root of the x, y, and z components of the spin structure factor, respectively.

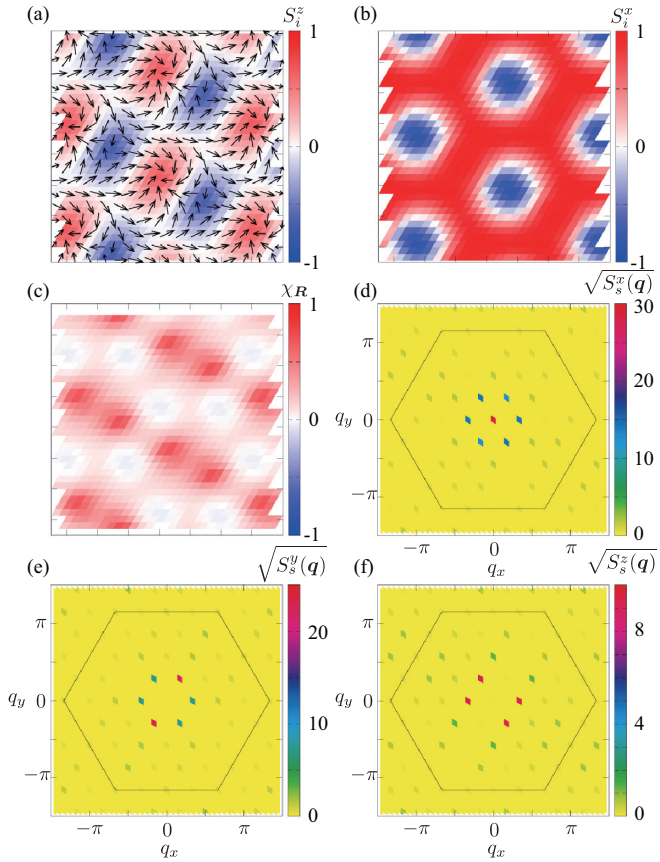

FIG. 5. Spin and chirality configurations of the SkX at $A = -0.2$ and $H^x = 1.0$. The contour shows the (a) z and (b) x components of the spin moment, and the arrows in (a) represent the xy components. In (c), the contour shows the scalar chirality. The square root of the (d) x, (e) y, and (f) z components of the spin structure factor, respectively.

The symmetry of the present in-plane SkX is different from that in frustrated magnets with easy-axis anisotropy in terms

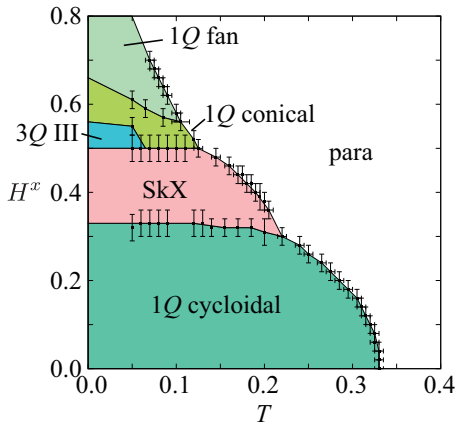

FIG. 6. The temperature-field phase diagram of the model in Eq. (1) obtained by Monte Carlo simulations at $J_3/|J_1| = 0.5$ and $A = -0.2$ for a system size with $N = 60^2$. The lines are guides for the eye.

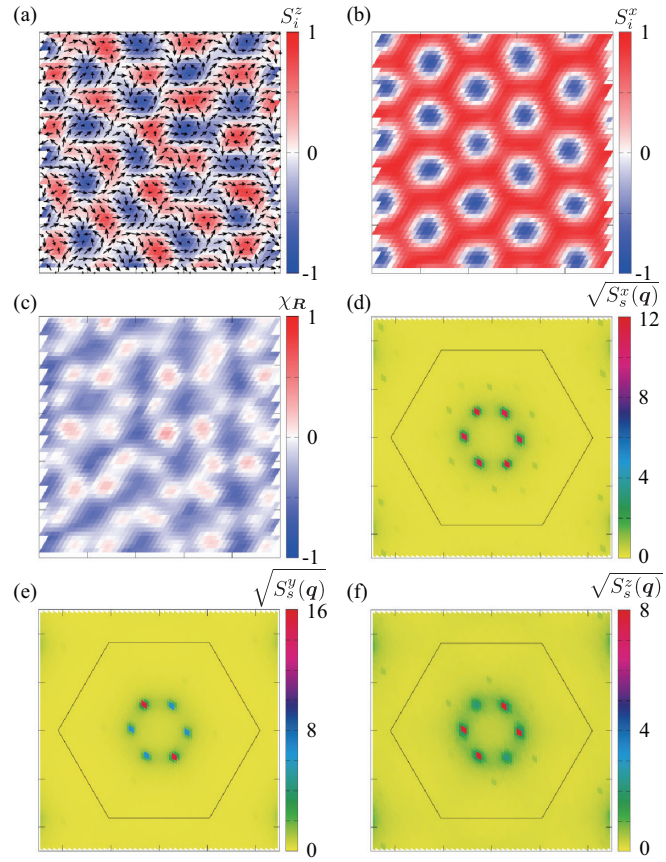

FIG. 7. Spin and chirality configurations of the SkX at $T = 0.175$, $A = -0.2$, and $H^x = 0.38$. The contour shows the (a) z and (b) x components of the spin moment, and the arrows in (a) represent the xy components. In (c), the contour shows the scalar chirality. The square root of the (d) x, (e) y, and (f) z components of the spin structure factor, respectively. The $\boldsymbol{q} = \boldsymbol{0}$ component of the spin structure factor is omitted for clarity.

of threefold rotational symmetry and that in chiral magnets with the DM interaction in terms of spatial inversion symmetry. Accordingly, it is expected to obtain different responses against an external ac field or current, which remains as a future issue. One of the candidate materials is the easy-plane triangular antiferromagnet $NiBr_2$ [74–76]. The other materials hosting an in-plane cycloidal spiral at zero field are also candidates for in-plane magnetic field-induced SkX. In the end, the SkX in frustrated magnets with easy-plane anisotropy will provide a potential application to spintronics devices owing to the different nature of that with easy-axis anisotropy [77,78] and that with the DM interaction.

ACKNOWLEDGMENTS

This research was supported by JSPS KAKENHI Grants No. JP19K03752, No. JP19H01834, No. JP21H01037, and by JST PREST (JPMJPR20L8). Parts of the numerical calculations were performed in the supercomputing systems in ISSP, the University of Tokyo.

[1] *Introduction to Frustrated Magnetism: Materials, Experiments, Theory*, edited by C. Lacroix, P. Mendels, and F. Mila, Springer Series in Solid-State Sciences (Springer, Berlin, 2011).
[2] P. W. Anderson, Mater. Res. Bull. **8**, 153 (1973).
[3] A. Kitaev, Ann. Phys. **321**, 2 (2006).
[4] L. Balents, Nature (London) **464**, 199 (2010).
[5] Y. Zhou, K. Kanoda, and T.-K. Ng, Rev. Mod. Phys. **89**, 025003 (2017).
[6] S. T. Bramwell and M. J. Gingras, Science **294**, 1495 (2001).
[7] C. Castelnovo, R. Moessner, and S. L. Sondhi, Nature (London) **451**, 42 (2008).
[8] J. S. Gardner, M. J. P. Gingras, and J. E. Greedan, Rev. Mod. Phys. **82**, 53 (2010).
[9] C. Nisoli, R. Moessner, and P. Schiffer, Rev. Mod. Phys. **85**, 1473 (2013).
[10] N. Laflorencie and F. Mila, Phys. Rev. Lett. **99**, 027202 (2007).
[11] P. Sengupta and C. D. Batista, Phys. Rev. Lett. **98**, 227201 (2007).
[12] V. Zapf, M. Jaime, and C. D. Batista, Rev. Mod. Phys. **86**, 563 (2014).
[13] P. Bak and M. H. Jensen, J. Phys. C: Solid State Phys. **13**, L881 (1980).
[14] D. H. Lee, J. D. Joannopoulos, J. W. Negele, and D. P. Landau, Phys. Rev. Lett. **52**, 433 (1984).
[15] L. Capriotti, A. E. Trumper, and S. Sorella, Phys. Rev. Lett. **82**, 3899 (1999).
[16] M. E. Zhitomirsky, Phys. Rev. Lett. **88**, 057204 (2002).
[17] T. Momoi, K. Kubo, and K. Niki, Phys. Rev. Lett. **79**, 2081 (1997).
[18] B. Binz and A. Vishwanath, Phys. Rev. B **74**, 214408 (2006).
[19] B. Binz, A. Vishwanath, and V. Aji, Phys. Rev. Lett. **96**, 207202 (2006).
[20] S.-Z. Lin, S. Hayami, and C. D. Batista, Phys. Rev. Lett. **116**, 187202 (2016).
[21] C. D. Batista, S.-Z. Lin, S. Hayami, and Y. Kamiya, Rep. Prog. Phys. **79**, 084504 (2016).
[22] H. Katsura, N. Nagaosa, and A. V. Balatsky, Phys. Rev. Lett. **95**, 057205 (2005).
[23] M. Mostovoy, Phys. Rev. Lett. **96**, 067601 (2006).
[24] Y. Tokura, S. Seki, and N. Nagaosa, Rep. Prog. Phys. **77**, 076501 (2014).
[25] S. Hayami, H. Kusunose, and Y. Motome, Phys. Rev. B **90**, 024432 (2014).
[26] K. Ohgushi, S. Murakami, and N. Nagaosa, Phys. Rev. B **62**, R6065 (2000).
[27] N. Nagaosa, J. Sinova, S. Onoda, A. H. MacDonald, and N. P. Ong, Rev. Mod. Phys. **82**, 1539 (2010).
[28] I. Martin and C. D. Batista, Phys. Rev. Lett. **101**, 156402 (2008).
[29] T. Kimura, Annu. Rev. Mater. Res. **37**, 387 (2007).
[30] A. N. Bogdanov and D. A. Yablonskii, Sov. Phys. JETP **68**, 101 (1989).
[31] A. Bogdanov and A. Hubert, J. Magn. Magn. Mater. **138**, 255 (1994).
[32] I. Dzyaloshinsky, J. Phys. Chem. Solids **4**, 241 (1958).
[33] T. Moriya, Phys. Rev. **120**, 91 (1960).
[34] U. K. Rößler, A. N. Bogdanov, and C. Pfleiderer, Nature (London) **442**, 797 (2006).
[35] S. D. Yi, S. Onoda, N. Nagaosa, and J. H. Han, Phys. Rev. B **80**, 054416 (2009).
[36] A. B. Butenko, A. A. Leonov, U. K. Rößler, and A. N. Bogdanov, Phys. Rev. B **82**, 052403 (2010).
[37] T. Okubo, S. Chung, and H. Kawamura, Phys. Rev. Lett. **108**, 017206 (2012).
[38] A. O. Leonov and M. Mostovoy, Nat. Commun. **6**, 8275 (2015).
[39] S.-Z. Lin and S. Hayami, Phys. Rev. B **93**, 064430 (2016).
[40] S. Hayami, S.-Z. Lin, and C. D. Batista, Phys. Rev. B **93**, 184413 (2016).
[41] I. Rousochatzakis, U. K. Rössler, J. van den Brink, and M. Daghofer, Phys. Rev. B **93**, 104417 (2016).
[42] S. Hayami, S.-Z. Lin, Y. Kamiya, and C. D. Batista, Phys. Rev. B **94**, 174420 (2016).
[43] S.-Z. Lin and C. D. Batista, Phys. Rev. Lett. **120**, 077202 (2018).
[44] Y. Hu, X. Chi, X. Li, Y. Liu, and A. Du, Sci. Rep. **7**, 16079 (2017).
[45] R. Ozawa, S. Hayami, and Y. Motome, Phys. Rev. Lett. **118**, 147205 (2017).
[46] S. Hayami, R. Ozawa, and Y. Motome, Phys. Rev. B **95**, 224424 (2017).
[47] S. Hayami and Y. Motome, Phys. Rev. B **99**, 094420 (2019).
[48] S. Hayami and Y. Motome, Phys. Rev. B **103**, 024439 (2021).
[49] S. Hayami and R. Yambe, J. Phys. Soc. Jpn. **90**, 073705 (2021).
[50] X. Zhang, J. Xia, Y. Zhou, X. Liu, H. Zhang, and M. Ezawa, Nat. Commun. **8**, 1717 (2017).
[51] J. Liang, J. Yu, J. Chen, M. Qin, M. Zeng, X. Lu, X. Gao, and J.-M. Liu, New J. Phys. **20**, 053037 (2018).
[52] X. Zhang, J. Xia, L. Shen, M. Ezawa, O. A. Tretiakov, G. Zhao, X. Liu, and Y. Zhou, Phys. Rev. B **101**, 144435 (2020).
[53] X. Yao, J. Chen, and S. Dong, New J. Phys. **22**, 083032 (2020).
[54] S. R. Saha, H. Sugawara, T. D. Matsuda, H. Sato, R. Mallik, and E. V. Sampathkumaran, Phys. Rev. B **60**, 12162 (1999).
[55] T. Kurumaji, T. Nakajima, M. Hirschberger, A. Kikkawa, Y. Yamasaki, H. Sagayama, H. Nakao, Y. Taguchi, T.-H. Arima, and Y. Tokura, Science **365**, 914 (2019).
[56] M. Hirschberger, T. Nakajima, S. Gao, L. Peng, A. Kikkawa, T. Kurumaji, M. Kriener, Y. Yamasaki, H. Sagayama, H. Nakao *et al.*, Nat. Commun. **10**, 5831 (2019).
[57] Y. Tokura and N. Kanazawa, Chem. Rev. **121**, 2857 (2020).
[58] M. Hirschberger, S. Hayami, and Y. Tokura, New J. Phys. **23**, 023039 (2021).
[59] B. Göbel, A. Mook, J. Henk, I. Mertig, and O. A. Tretiakov, Phys. Rev. B **99**, 060407(R) (2019).
[60] K.-W. Moon, J. Yoon, C. Kim, and C. Hwang, Phys. Rev. Applied **12**, 064054 (2019).
[61] L. Flacke, V. Ahrens, S. Mendisch, L. Körber, T. Böttcher, E. Meidinger, M. Yaqoob, M. Müller, L. Liensberger, A. Kákay *et al.*, arXiv:2102.11117.
[62] L. Shen, X. Li, J. Xia, L. Qiu, X. Zhang, O. A. Tretiakov, M. Ezawa, and Y. Zhou, Phys. Rev. B **102**, 104427 (2020).
[63] M. Finazzi, M. Savoini, A. R. Khorsand, A. Tsukamoto, A. Itoh, L. Duò, A. Kirilyuk, T. Rasing, and M. Ezawa, Phys. Rev. Lett. **110**, 177205 (2013).
[64] M. Beg, R. Carey, W. Wang, D. Cortés-Ortuño, M. Vousden, M.-A. Bisotti, M. Albert, D. Chernyshenko, O. Hovorka, R. L. Stamps *et al.*, Sci. Rep. **5**, 17137 (2015).
[65] W. Koshibae and N. Nagaosa, Nat. Commun. **7**, 10542 (2016).

[66] F. Hellman, A. Hoffmann, Y. Tserkovnyak, G. S. D. Beach, E. E. Fullerton, C. Leighton, A. H. MacDonald, D. C. Ralph, D. A. Arena, H. A. Dürr *et al.*, Rev. Mod. Phys. **89**, 025006 (2017).
[67] S. Hayami and Y. Motome, Phys. Rev. B **103**, 054422 (2021).
[68] A. H. Bobeck and H. Scovil, Sci. Am. **224**, 78 (1971).
[69] A. A. Thiele, Phys. Rev. Lett. **30**, 230 (1973).
[70] R. Seshadri and R. M. Westervelt, Phys. Rev. Lett. **66**, 2774 (1991).
[71] Y. Su, S. Hayami, and S.-Z. Lin, Phys. Rev. Research **2**, 013160 (2020).
[72] S. Hayami, J. Magn. Magn. Mater. **513**, 167181 (2020).
[73] S. Seo, S. Hayami, Y. Su, S. M. Thomas, F. Ronning, E. D. Bauer, J. D. Thompson, S.-Z. Lin, and P. F. Rosa, Commun. Phys. **4**, 58 (2021).
[74] P. Day, A. Dinsdale, E. Krausz, and D. Robbins, J. Phys. C **9**, 2481 (1976).
[75] B. K. Rai, A. D. Christianson, D. Mandrus, and A. F. May, Phys. Rev. Materials **3**, 034005 (2019).
[76] S. Babu, K. Prokeš, Y. Huang, F. Radu, and S. Mishra, J. Appl. Phys. **125**, 093902 (2019).
[77] S. K. Kim, Phys. Rev. B **99**, 224406 (2019).
[78] L. Shen, J. Xia, X. Zhang, M. Ezawa, O. A. Tretiakov, X. Liu, G. Zhao, and Y. Zhou, Phys. Rev. Lett. **124**, 037202 (2020).